A. Appendix

We present criteria for loss functions and an overview of metrics in Section A.1. We propose more details about the architectures in Sec. A.2, and present more results in Sec. A.3. Sec. A.4 describes a dataset-specific feature embedding analysis.

A.1. Loss Functions

In the following, we state all loss functions that we used for our methodology. We describe the cross-entropy loss for the Multivariate Time Series Classification (MTSC) task. Next, we present criteria for the trajectory regression task. Finally, we propose *distance*-based, *spatio-temporal* and *distribution*-based loss functions.

MTSC Task: Cross-entropy Loss. For the MTSC task, the cross-entropy loss [25] is defined by

$$\mathcal{L}_{CE}(\mathcal{U}, \mathcal{V}) = -\frac{1}{n}\sum_{i=1}^{n} v_i \log \hat{v}_i, \tag{2}$$

where the Multivariate Time Series (MTS) $\mathbf{U} = \{\mathbf{u}_1, \ldots, \mathbf{u}_m\} \in \mathbb{R}^{m \times l}$ is an ordered sequence of $m \in \mathbb{N}$ streams with $\mathbf{u}_i = (u_{i,1}, \ldots, u_{i,l}), i \in \{1, \ldots, m\}$. m is the length of the time series and l is the number of dimensions. Each MTS is associated with a class label $v \in \Omega$ from a pre-defined label set Ω. The training set is a subset of the array $\mathcal{U} = \{\mathbf{U}_1, \ldots, \mathbf{U}_n\} \in \mathbb{R}^{n \times m \times l}$, where n is the number of time series, and the corresponding labels $\mathcal{V} = \{v_1, \ldots, v_n\} \in \Omega^n$ [60]. The MTSC task is to predict an unknown class label $\hat{\mathcal{V}}$ for a given MTS.

Trajectory Regression Task: Criteria. For the trajectory regression task it is given a ground truth time series $\mathcal{Y} = \{\mathbf{y}_1, \ldots, \mathbf{y}_m\} \in \mathbb{R}^{m \times d}$. The goal is to predict a time series $\mathcal{X} = \{\mathbf{x}_1, \ldots, \mathbf{x}_n\} \in \mathbb{R}^{n \times d}$, such that $\mathcal{X}$ is closely aligned to $\mathcal{Y}$. In the following, we consider $\mathbf{r}_i = \mathbf{y}_i - \mathbf{x}_i$ be the residual between $\mathcal{X}_i$ and $\mathcal{Y}_i$. We consider a (differentiable) substitution-cost function $\mathcal{L} : \mathbb{R}^d \times \mathbb{R}^d \rightarrow \mathbb{R}_+$ to learn the trajectory regression task. All metrics to be used in a neural network have to obey the following criteria, where $\mathcal{X}, \mathcal{Y}, \mathcal{Z} \in \mathbb{R}$ [34]:

$$\mathcal{L}(\mathcal{X}, \mathcal{Y}) \geq 0 \;\; \text{(non-negativity)} \tag{I}$$

$$\mathcal{L}(\mathcal{X}, \mathcal{Y}) = \mathcal{L}(\mathcal{Y}, \mathcal{X}) \;\; \text{(symmetry)} \tag{II}$$

$$\mathcal{L}(\mathcal{X}, \mathcal{Y}) \leq \mathcal{L}(\mathcal{X}, \mathcal{Z}) + \mathcal{L}(\mathcal{Z}, \mathcal{Y}) \;\; \text{(triangle inequ.)} \tag{III}$$

$$\mathcal{L}(\mathcal{X}, \mathcal{Y}) = 0 \Leftrightarrow \mathcal{X} = \mathcal{Y} \;\; \text{(ident. of indiscernibles)} \tag{IVa}$$

It is difficult to make accurate predictions about the injectivity as floating points operations and approximation errors lead to a distance of zero for slightly different inputs.

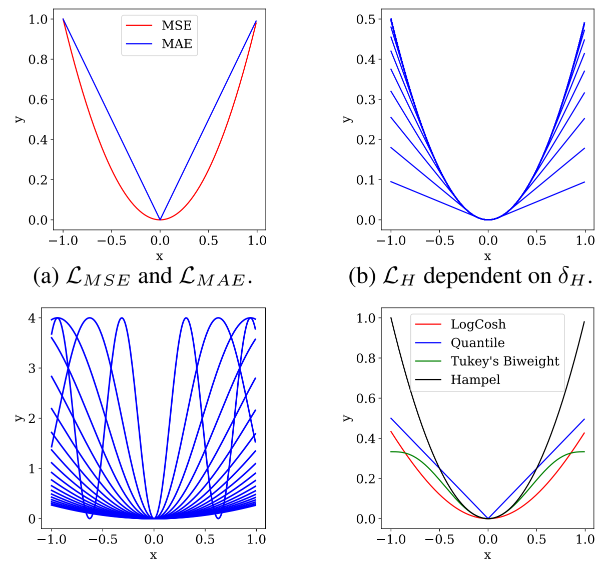

(a) $\mathcal{L}_{MSE}$ and $\mathcal{L}_{MAE}$. (b) $\mathcal{L}_H$ dependent on δ_H. (c) $\mathcal{L}_{AS}$ loss dependent on δ_{AS}. (d) Other loss functions.

Figure 10: Sample weighting based on different *distance*-based metrics.

Hence, Equ. (IVa) can be formulated as a *pseudometric* with a relaxed identity of indiscernibles where $\tilde{\mathcal{X}} \in \mathbb{R}$:

$$\mathcal{L}(\tilde{\mathcal{X}}, \tilde{\mathcal{X}}) = 0. \tag{IVb}$$

Trajectory Regression Task: Distance-based Loss Functions. We consider the Mean Squared Error

$$\mathcal{L}_{MSE}(\mathcal{X}, \mathcal{Y}) = \frac{1}{n}\|\mathcal{Y} - \mathcal{X}\|_2^2 = \frac{1}{n}\sum_{i=i}^{n} \mathbf{r}_i^2 \tag{3}$$

with L_2-norm $||\cdot||_2$ (see Fig. 10a). The derivative of the $\mathcal{L}_{MSE}$ loss is $\frac{\partial}{\partial \mathcal{X}}\mathcal{L}_{MSE}(\mathcal{X}, \mathcal{Y}) = -\frac{2}{n}\sum_{i=i}^{n} \mathbf{r}_i$. The Mean Absolute Error (MAE) is

$$\mathcal{L}_{MAE}(\mathcal{X}, \mathcal{Y}) = \frac{1}{n}\|\mathcal{Y} - \mathcal{X}\|_1 = \frac{1}{n}\sum_{i=i}^{n} |\mathbf{r}_i| \tag{4}$$

with the L_1-norm $||\cdot||_1$. Its derivative is $\frac{\partial}{\partial \mathcal{X}}\mathcal{L}_{MAE}(\mathcal{X}, \mathcal{Y}) = 1/n\sum_{i=i}^{n} \text{sign}(\mathbf{r}_i)$. The Huber loss [30]

$$\mathcal{L}_H(\mathcal{X}, \mathcal{Y}, \delta_H) = \sum_{i:|\mathbf{r}_i| \leq \delta_H}^{n} \frac{1}{2}(\mathbf{r}_i)^2 + \sum_{i:|\mathbf{r}_i| > \delta_H}^{n} \delta_H|\mathbf{r}_i| - \frac{1}{2}\delta_H^2 \tag{5}$$

is less sensitive to outliers, but depends on the hyperparameter δ_H (see Fig. 10b). The derivative of the Huber loss is

$$\frac{\partial}{\partial \mathcal{X}}\mathcal{L}_H(\mathcal{X}, \mathcal{Y}, \delta_H) = -\sum_{i:|\mathbf{r}| \leq \delta_H}^{n} \mathbf{r}_i - \sum_{i:|\mathbf{r}_i| > \delta_H}^{n} \delta_H \text{sign}(\mathbf{r}_i). \tag{6}$$

Similar, the Andrew's Sine loss [8] is

$$\mathcal{L}_{AS}(\mathcal{X},\mathcal{Y},\delta_{AS}) = \sum_{i:|\mathbf{r}_i|\leq 1}^{n} 4sin\left(\frac{\mathbf{r}_i}{2\delta_{AS}}\right)^2 + \sum_{i:|\mathbf{r}_i|>1}^{n} 1, \tag{7}$$

with hyperparameter δ_{AS} (see Fig. 10c) with the derivative

$$\frac{\partial}{\partial \mathcal{X}}\mathcal{L}_{AS}(\mathcal{X},\mathcal{Y},\delta_{AS}) = \sum_{i:|\mathbf{r}|\leq 1}^{n} \frac{2}{\delta_{AS}} sin\left(\frac{\mathbf{r}_i}{\delta_{AS}}\right). \tag{8}$$

Trajectory Regression Task: Spatio-temporal Loss Functions. We define the Cosine Similarity by

$$\mathcal{L}_{CS}(\mathcal{X},\mathcal{Y}) = 1 - \frac{\mathbf{x}\cdot\mathbf{y}}{\|\mathbf{x}\|_2\|\mathbf{y}\|_2}. \tag{9}$$

The Cosine Similarity is a proper metric as it satisfies the requirements $\mathcal{L}_{CS}(\mathcal{X},\mathcal{Y}) \geq 0$ (I), $\mathcal{L}_{CS}(\mathcal{X},\mathcal{Y}) = \mathcal{L}_{CS}(\mathcal{Y},\mathcal{X})$ (II), and $\mathcal{L}_{CS}(\mathcal{X},\mathcal{X}) = 0$ (IVb). Under certain conditions the triangle equality (III) is not fulfilled [36]. This loss function is a measure of similarity between two non-zero vectors of an inner product space, but is not invariant to shifts. The Pearson Correlation loss [47] $\mathcal{L}_{PC}(\mathcal{X},\mathcal{Y}) = \mathcal{L}_{CS}(\mathcal{X}-\overline{\mathcal{X}},\mathcal{Y}-\overline{\mathcal{Y}})$, in contrast, is invariant to shifts. This means, when $\mathcal{X}$ is transformed by $a+b\mathcal{X}$ and $\mathcal{Y}$ is transformed by $c+d\mathcal{Y}$, where a,b,c and d are constants ($b,d>0$), the Pearson Correlation coefficient is invariant in location and scale in the two variables. The Pearson Correlation loss is defined by

$$\mathcal{L}_{PC}(\mathcal{X},\mathcal{Y}) = 1 - \frac{s_{xy}}{s_x\cdot s_y} = 1 - \frac{(\mathbf{x}-\overline{\mathbf{x}})\cdot(\mathbf{y}-\overline{\mathbf{y}})}{\|\mathbf{x}-\overline{\mathbf{x}}\|_2\|\mathbf{y}-\overline{\mathbf{y}}\|_2}. \tag{10}$$

with the sample mean $\overline{\mathbf{x}} = \frac{1}{n}\sum_{i=1}^{n}\mathbf{x}_i$. Analogously for $\overline{\mathbf{y}}$. The covariance is $s_{xy} = \frac{1}{n}(\mathbf{x}-\overline{\mathbf{x}})\cdot(\mathbf{y}-\overline{\mathbf{y}})$, and the variance of the features is $s_x^2 = \frac{1}{n}\sum_{i=1}^{n}(\mathbf{x}_i-\overline{\mathbf{x}})^2$, analogously for s_y^2. The partial derivative of the Pearson Correlation [54] regarding $\mathbf{x}$ is

$$\frac{\partial}{\partial \mathbf{x}}\mathcal{L}_{PC}(\mathcal{X},\mathcal{Y}) = \frac{(\mathbf{y}-\overline{\mathbf{y}}) - \frac{s_{xy}}{s_y}\cdot(\mathbf{x}-\overline{\mathbf{x}})}{s_x\cdot s_y}. \tag{11}$$

Further alternative *distance*-based metrics are, e.g., the LogCosh, the Quantile [45], the Tukey's Biweight [7], the Hampel [8] and the Geman McClure metric [6] (see Fig. 10d). For more information, see [37] for *distance*-based metrics and [52] for *spatio-temporal* metrics.

Trajectory Regression Task: Distribution-based Loss Functions. We use the *distribution*-based loss function, i.e., the Wasserstein distance [23], defining a distance between two probability distributions on a given metric space $\mathcal{M}$ and representing the cost δ of an optimal mass transportation problem. Optimal transport can be used to compare probability measures in metric spaces. There exists some $\mathcal{X}_0$ in $\mathcal{M}$ such that the Wasserstein space of order p is defined as

$$P_p(\mathcal{M}) := \Big\{\mu \in P(\mathcal{M});\ \int_{\mathcal{M}} \delta(\mathcal{X},\mathcal{X}_0)^p d\mathcal{X} < \infty\Big\}. \tag{12}$$

The p^{th} Wasserstein distance between two probability measures μ and ν is defined as

$$\begin{aligned} W_p(\mu,\nu) &:= \left(\inf_{\gamma\in\Gamma(\mu,\nu)} \int_{\mathcal{M}\times\mathcal{M}} \delta(\mathcal{X},\mathcal{Y})^p d\gamma(\mathcal{X},\mathcal{Y})\right)^{\frac{1}{p}} \\ &= \inf\Big\{\left[\mathbb{E}[d(X,Y)^p]\right]^{\frac{1}{p}},\ \text{law}(X)=\mu,\ \text{law}(Y)=\nu\Big\}, \end{aligned} \tag{13}$$

with the collection of all probability measures $\Gamma(\mu,\nu)$ on $\mathcal{M}\times\mathcal{M}$ and $p\in[1,\infty)$. $\mathbb{E}[X]$ denotes the expected value of a random variable X. We consider the classical case where the metric is the Euclidean metric in space $\mathbb{R}^d \subset \mathcal{M}$, and hence, $\delta(\mathcal{X},\mathcal{Y}) = ||\mathcal{X}-\mathcal{Y}||$. For all subsets $P\subset\mathbb{R}^d$, we have $\gamma(P\times\mathbb{R}^d) = \mu(P)$ and $\gamma(P\times\mathbb{R}^d) = \nu(P)$. [48] The W_1 distance is also called the Kantorovich-Rubinstein distance. The Wasserstein distance satisfies the criteria (I) to (IVa): It holds the non-negativity criteria $W_p(\mu,\nu)\geq 0$ (I), and the symmetry criteria $W_p(\mu,\nu) = W_p(\nu,\mu)$ (II). Assume that $W_p(\nu,\mu) = 0$, then there exists a transference plan that is concentrated on the diagonal, and it holds $\mathcal{X}=\mathcal{Y}$ (IVa). Furthermore, let μ_1, μ_2 and μ_3 be probability measures on $\mathcal{M}\times\mathcal{M}$, and (T_1,T_2), respectively (Q_2,Q_3), be an optimal coupling of (μ_1,μ_2), respectively of (μ_2,μ_3). There exist random variables $(T_1^{'},T_2^{'},T_3^{'})$ with $\text{law}(T_1^{'},T_2^{'}) = \text{law}(T_1,T_2)$ and $\text{law}(T_2^{'},T_3^{'}) = \text{law}(Q_2,Q_3)$, such that

$$\begin{aligned} W_p(\mu_1,\mu_3) &\leq \left(\mathbb{E}[d(T_1^{'},T_3^{'})^p]\right)^{\frac{1}{p}} \leq \\ &\leq \left(\mathbb{E}[d(T_1^{'},T_2^{'}) + d(T_2^{'},T_3^{'})]^p\right)^{\frac{1}{p}} \leq \\ &\leq \left(\mathbb{E}[d(T_1^{'},T_2^{'})^p]\right)^{\frac{1}{p}} + \left(\mathbb{E}[d(T_2^{'},T_3^{'})^p]\right)\right)^{\frac{1}{p}} = \\ &= W_p(\mu_1,\mu_2) + W_p(\mu_2,\mu_3), \end{aligned} \tag{14}$$

and the triangle inequality holds (III). The duality formula for the Kantorovich-Rubinstein distance is

$$W_1(\mu,\nu) = \sup_{||\psi||_{Lip}\leq 1}\left\{\int_{\mathcal{M}}\psi d\mu \int_{\mathcal{M}}\psi d\nu\right\}, \tag{15}$$

for any μ,ν in the Wasserstein space $P_1(\mathcal{M})$. The Wasserstein distance W_1 of order 1 is the weakest of all, and hence, is easier to bound. The Wasserstein distance has the ability to capture weak convergence precisely and are rather strong as they take care of large distances in $\mathcal{M}\times\mathcal{M}$. [57] For more information, see [43].

Summary. For the classification task, we use the $\mathcal{L}_{CE}$ loss function (2). For the regression task, we use a combination of the *distance*-based loss functions $\mathcal{L}_{MSE}$ (3), $\mathcal{L}_{MAE}$

Network	Total	Trunk	Regr.	Class.
Only regression (A_0)	117,052	96,852	20,200	-
Only classification (A_1)	133,735	117,051	-	16,683
Class. for regr. (A_2)	190,535	117,052	56,800	16,683
Latest split (A_3)	133,735	96,852	20,200	16,683
Late split (A_4)	153,935	96,852	20,200	36,883
Split after LSTM (A_5)	194,935	86,352	30,700	77,883
Split after 2. Drop. (A_6)	260,935	20,352	96,700	143,883
Split after 1. Drop. (A_7)	277,639	3,648	113,404	160,587
Separate heads (A_8)	281,287	0	117,052	164,235

Table 5: Parameters of the inertial-based models.

Network	Total	Trunk	Regr.	Class.
Only regression (A_0)	1,342,638	1,322,438	20,200	-
Only classification (A_1)	1,359,321	1,342,638	-	16,683
Class. for regr. (A_2)	1,416,121	1,342,638	56,800	16,683
Latest split (A_3)	1,359,321	1,355,804	20,200	16,683
Late split (A_4)	1,379,521	1,322438	20,200	36,883
Split after 1. LSTM (A_5)	1,619,921	1,082,038	260,600	277,283
LSTM in traj. head (A_6)	1,459,521	1,082,038	260,600	116,883
LSTM in class. head (A_7)	1,459,521	982,038	100,200	377,283
Split after 1. Drop. (A_8)	2,701,959	76	1,342,600	1,359,283

Table 6: Parameters of the visual-based models.

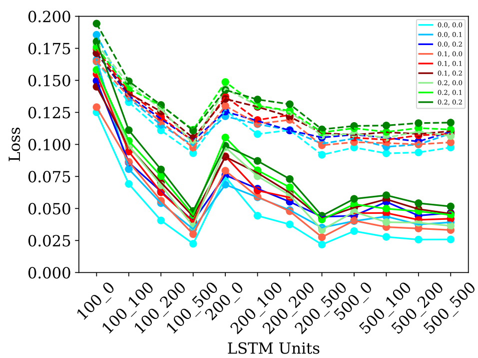

Figure 11: Grid search for an optimal number of LSTM units and dropout for the visual-based CNN. Continuous line: training loss. Dashed line: validation error.

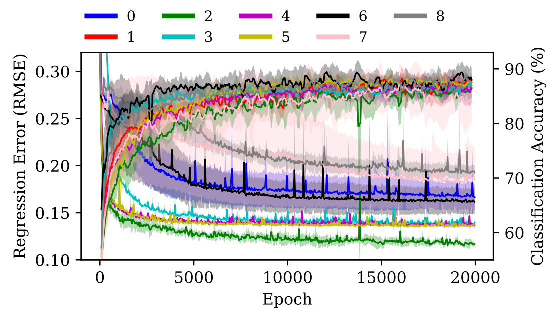

Figure 12: Evaluation for CNN architectures (A_0-A_8) trained with the $\mathcal{L}_{MSE}$ and $\mathcal{L}_{CE}$ loss averaged over all trainings.

(4), $\mathcal{L}_H$ (5) and $\mathcal{L}_{AS}$ (7), *spatio-temporal* loss functions $\mathcal{L}_{CS}$ (9) and $\mathcal{L}_{PC}$ (10), and the *distribution-based* Wasserstein function $\mathcal{L}_{WAS_p}$ (13).

A.2. MTL Network Architectures

The general overview of the framework is given in Fig. 2 (Sec. 3). The input is for the IMU-based and the visual-based *OnHW* dataset a MTS that differs regarding its input size. For the IMU-based dataset, the input are the 13 channels of the accelerometers, gyroscope, magnetometer and force sensor. The number of timesteps depends on the sample length. For the visual dataset, the input is the two dimensional trajectory of the pen tip in camera coordinates. What follows, is a CNN trunk, a classification head, and a regression head. The classification head is used for the MTSC task by predicting a class label with the cross-entropy loss. The regression head is used for the trajectory regression task that predicts a MTS that represents the trajectory of the written character. The loss function for this task is a combination of *distance*-based, *spatio-temporal*, and *distribtuion*-based metrics.

The number of trainable parameters in the neural network trunk and in task-specific heads is important. We address the problem in the following. We construct for each dataset nine architectures with different split points. Architectures A_0 and A_1 are Single Task Learning (STL) CNNs for the MTSC task and the trajectory prediction task. Architectures A_2 to A_8 combine both tasks by MTL. All IMU-based architectures are given in Fig. 3. All visual-based architectures are given in Fig. 4, where we search for the optimal number of LSTM units and dropouts (see Fig. 11). We choose a combination of 500 and 100 LSTM units, and two dropout layers of 20%. An overview of all architectures and its number of trainable parameters is given in Table 5 and in Table 6. The number of total parameters increases for an early split point compared to late split points for both networks. A regression head with one *dense* layer of 200 neurons has 20,200 parameters, while a classification head with one *dense* layer of 83 neurons has 16,683 parameters. Fig. 12 compares the training loss of all architectures for the regression and classification tasks.

A.3. Evaluation Results

Hyperparameter Search for the Inertial-based Architectures. For the alternative *distance*-based metrics, i.e., Andrew's Sine and Huber, we search for the hyperparameters δ_H and δ_{AS} in $\{0.1, 0.2, \dots, 2.0, 2.5, \dots, 5.0\}$ using a grid search (Fig. 14a). For $\mathcal{L}_{AS}$ we choose $\delta_{AS} = 0.3$, and for $\mathcal{L}_H$ we choose $\delta_H = 4.0$ for follow-up training. A large δ_H tends to weight outliers more, while a small outlier rejection has a higher standard deviation. We also search for the hyperparameter $p \in \{1, 2, 3, 4\}$ of the *distribution*-based loss $\mathcal{L}_{WAS_p}$ (Fig. 14a) and choose $p = 1$ for follow-up training.

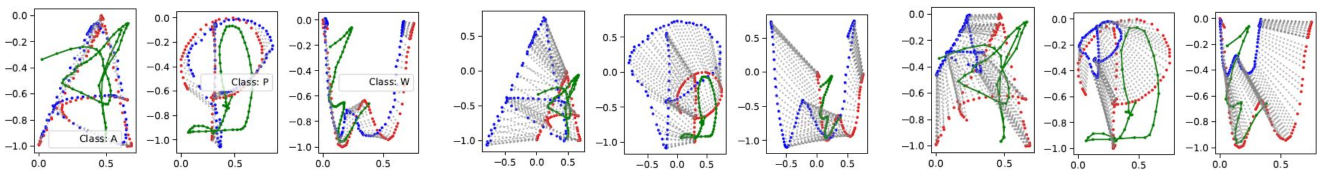

(a) MSE. (b) Pearson Correlation. (c) Cosine Similarity.

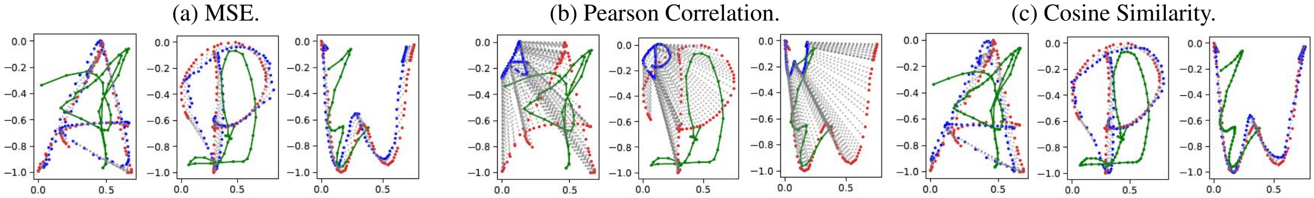

(d) MSE + Pearson Correlation. (e) MSE and Cosine Similarity. (f) MSE + Wasserstein distance.

Figure 13: Trajectory prediction (blue) against the ground truth trajectory (red) of the characters `'A'`, `'P'` and `'W'` based on visual data (green) as MTS input preprocessed with U-Net [49].

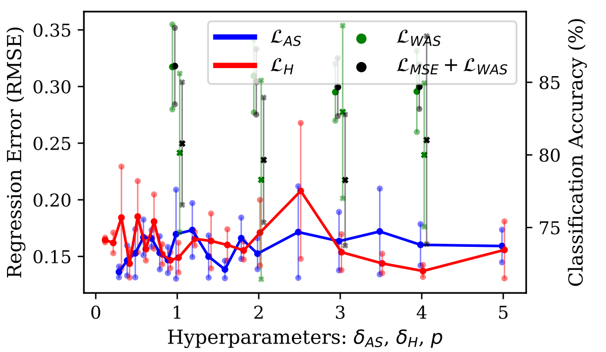

(a) Inertial dataset.

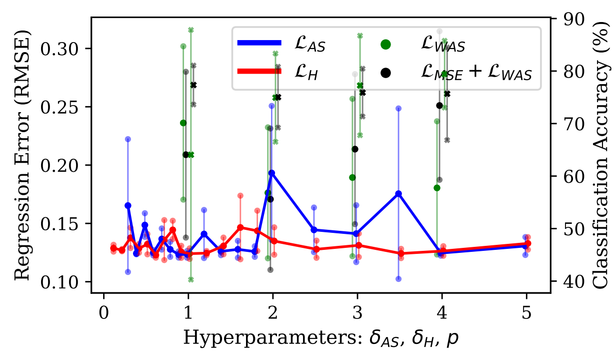

(b) Visual dataset.

Figure 14: Grid search for δ_{AS}, δ_H and p averaged over all architectures. For $\mathcal{L}_{WAS_p}$: left: trajectory error, right: classification accuracy.

Hyperparameter Search for Visual-based Architectures. As for the inertial-based architectures, we search for the optimal hyperparameter of alternative distance-based metrics using a grid search (see Fig. 14b). For $\mathcal{L}_{AS}$ we choose $\delta_{AS} = 2.5$, and for $\mathcal{L}_H$ we choose $\delta_H = 2.0$ for follow-up training. We also search for the hyperparameter p in the *distribution*-based loss $\mathcal{L}_{WAS_p}$ and choose $p = 4$ for follow-up training as it achieves the highest classification accuracy for both the single $\mathcal{L}_{WAS_4}$ loss and the combination of $\mathcal{L}_{MSE}$ and $\mathcal{L}_{WAS_4}$.

Loss function	IMU-based CNN	Visual-based CNN
$\mathcal{L}_{MSE}$	0.3052 ± 0.0401	5.8961 ± 0.0533
$\mathcal{L}_{H}$	0.2971 ± 0.0401	5.8154 ± 0.1067
$\mathcal{L}_{AS}$	0.2993 ± 0.0399	5.8349 ± 0.1259
$\mathcal{L}_{PC}$	0.3027 ± 0.0394	4.4017 ± 0.0924
$\mathcal{L}_{CS}$	0.3001 ± 0.0395	4.4246 ± 0.0488
$\mathcal{L}_{WAS_1}$	0.2994 ± 0.0395	4.4538 ± 0.0996
$\mathcal{L}_{MSE} + \mathcal{L}_{PC}$	0.3078 ± 0.0397	5.9077 ± 0.0610
$\mathcal{L}_{MSE} + \mathcal{L}_{CS}$	0.2984 ± 0.0387	5.8790 ± 0.1133
$\mathcal{L}_{MSE} + \mathcal{L}_{WAS_1}$	0.3096 ± 0.0396	5.9607 ± 0.1253

Table 7: Overview of inference times in seconds (s) (mean and standard deviation over all epochs) for architecture A_0.

Camera-based reconstruction. In Fig. 13 we propose additional trajectory reconstruction results based on the visual dataset. We come to similar conclusions as for the inertial-based dataset. While the CNN trained with the $\mathcal{L}_{MSE}$ loss combined with the $\mathcal{L}_{PC}$ loss (Fig. 13d) predicts a smoother trajectory than the single *distance*-based loss functions (Fig. 13a), the $\mathcal{L}_{MSE} + \mathcal{L}_{WAS}$ loss allows a proper training (Fig. 13f).

Training Times. For all loss combinations, we present inference times (Table 7). While the visual-based CNN takes 5.3971s for each epoch (on average), the IMU-based CNN only takes 0.3022s. The differences between the loss functions are small for the IMU-based architectures. From the visual-based CNNs we can see that the *spatio-temporal* and *distribution*-based loss functions (4.4267s) are less computive-intense compared to the *distance*-based loss functions (5.8488s). The marginally increased computing time for all loss combinations (5.9158s) is negligible.

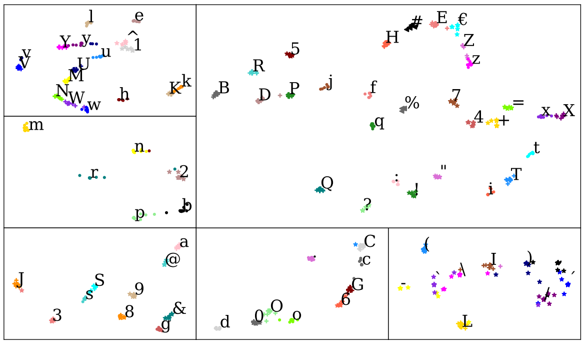

Figure 15: Visualization of the network embedding of the last layer based on the t-SNE algorithm by [56].

A.4. Dataset Feature Embedding Evaluation

Fig. 15 illustrates the challenges of the inertial dataset using a 300 dimensional feature embedding. The figure represents the feature embedding based on the t-SNE algorithm [56] (initial dimension of 301, perplexity of 30, an initial momentum of 0.5, and a final momentum of 0.8) and incorporates all 83 classes, i.e., capital and small characters, numbers and symbols. As it can be seen, the classes can be well separated. The main difficulty is to differentiate capital and small letters, e.g., `'V'` and `'v'`, `'K'` and `'k'`, and `'X'` and `'x'`, as these differ only in the size and not in the number of strokes. Naturally, the embeddings of the letters `'O'`, `'o'` and `'0'` are very close to each other. Furthermore, the classes `'G'`, `'6'`, `'C'`, `'c'` and `'('` are challenging to distinguish. These are one of the most frequent errors of the networks for the MTSC task.